SURFACE AND INTERFACE ANALYSIS
Surf. Interface Anal. **27**, 941–949 (1999)

XPS Analysis and Microstructural Characterization of a Ce/Tb Mixed Oxide Supported on a Lanthana-modified Transition Alumina

A. Galtayries,[1]* G. Blanco,[2] G. A. Cifredo,[2] D. Finol,[2] J. M. Gatica,[2] J. M. Pintado,[2] H. Vidal,[2] R. Sporken[1] and S. Bernal[2]

[1] Laboratoire Interdisciplinaire de Spectroscopie Electronique (LISE), Facultés Universitaires Notre-Dame de la Paix, B-5000 Namur, Belgium

[2] Departamento de Ciencia de los Materiales e Ingeniería Metalúrgica y Quimica Inorgánica, Facultad de Ciencias, Universidad de Cádiz, Aptdo. 40-Puerto Real, 11510 Cádiz, Spain

In the framework of a research project aimed at developing alternative materials for application in three-way catalysis, this work reports on the preparation and characterization of a ceria–terbia mixed oxide supported on a lanthana-modified transition alumina. This complex multicomponent oxide system has been characterized by combining x-ray diffraction (XRD), high-resolution electron microscopy (HREM), temperature-programmed desorption mass spectrometry (TPD-MS), Fourier transform infrared spectroscopy (FTIR) and x-ray photoelectron spectroscopy (XPS). Following a dry impregnation procedure, the lanthana-containing phase was deposited first, the ceria–terbia oxide being dispersed on the modified alumina in a subsequent step. The structural and chemical characterization studies carried out on the La_2O_3/Al_2O_3 binary system provide no evidence of a crystalline lanthana-containing phase. Neither lanthanum oxide nor the phases resulting from its aging in air could be identified. Likewise, no lanthana–alumina mixed oxide phases could be deduced from analysis of the HREM micrographs, selected-area electron diffraction (SAED) or XRD patterns. As deduced from the H_2O and CO_2 TPD studies, the chemisorptive properties of the La_2O_3/Al_2O_3 are significantly different from those of the alumina and the bulk lanthana. We conclude, accordingly, that the supported lanthana consists of a highly dispersed oxide in strong interaction with the alumina support. By contrast, after deposition and further calcination of the cerium–terbium nitrate precursors, the presence of fluorite microcrystals of average size 5 nm could be identified both by XRD and HREM.

The XPS studies carried out on the alumina support, La_2O_3/Al_2O_3 and $CeTbO_x/La_2O_3/Al_2O_3$, as well as a series of reference systems consisting of aged-in-air lanthana, $CeLaO_x$ and $CeTbO_x$ mixed oxides, have revealed the presence in the ternary system ($CeTbO_x/La_2O_3/Al_2O_3$) of at least two different types of chemical environments for the lanthanum ions. With the help of the La $3d_{5/2}$ spectra recorded for the different reference systems, we conclude that these two environments correspond to highly dispersed lanthana strongly interacting with OH^- and/or CO_3^{2-} groups, and to La^{3+} species incorporated in the Ce/Tb mixed oxide phase.

KEYWORDS: XPS; HREM; XRD; cerium/terbium mixed oxide; TWC

INTRODUCTION

Lanthanide oxides are finding very interesting applications in environmental catalysis.[1,2] In particular, ceria[1,3–5] and, more recently, ceria-based mixed oxides[1,6,7] are key components of the three-way catalysts (TWCs) used nowadays for controlling the exhaust emissions from spark-ignited motor vehicles. Among several other relevant functions, these oxides play an essential role as buffers of the fast oxygen pressure oscillations occurring in the exhaust gases while running the vehicles.[8]

Among the new redox materials for TWC applications, Ce/Zr mixed oxides are by far the most extensively investigated. Compared with pure ceria, the Ce/Zr oxides show better oxygen storage capacity (OSC),[9,10] oxygen buffering capacity (OBC)[11] and enhanced low-temperature reducibility.[12] Likewise, they exhibit a much better chemical[13,14] and textural[15,16] response to the high-temperature ageing processes that the TWCs suffer under real operation conditions. Although to a much lesser extent, several other modified cerias, all of them with fluorite structure, have been investigated as TWC alternative materials. In particular, some data are presently available on ceria-doped La,[17] Pr,[18,19] Y[17] and Hf[7] oxides.

Very recently, results on the redox properties of a ceria/terbia mixed oxide have also been reported.[20,21] In accordance with these results, this oxide shows and

* Correspondence to: A. Galtayries, Laboratoire de Physico-Chimie des Surfaces, ENSP, 11 rue Pierre et Marie Curie, 75231 Paris Cedex 05, France.

Contract/grant sponsor: EU; Contract/grant number: ERB FMRX-CT96-0060.

Contract/grant sponsor: Belgian Fund for Scientific Research.

CCC 0142–2421/99/100941–09 $17.50

Received 2 April 1999
Revised 7 June 1999; Accepted 7 June 1999

outstanding behaviour. Thus, the OBC of the bare Ce/Tb oxide at moderate temperatures ($T \leq 773$ K) is much better than that exhibited by ceria, and even by a ceria-supported Rh catalyst with rather similar textural properties.[21] Also worth noting is the very wide range of temperatures in which the mixed oxide shows good redox activity, this being the case in spite of its low surface area.[20] All these previous results prompted us to initiate a research project aimed at investigating the behaviour of this Ce/Tb mixed oxide dispersed on a conventional TWC support: a transition alumina. Prior to deposition of the mixed oxide, the alumina surface was modified by adding lanthana. As is already known[22,23] the lanthana improves the textural stability of the transition aluminas. Likewise, it was expected that the surface modification of the alumina by lanthana would prevent stabilization of the trivalent Ce (Tb) ions through the formation of a surface mixed phase, $LnAlO_3$ (Ln = Ce, Tb), with inherent loss of redox efficiency in the supported mixed oxide.[24]

In this work, we shall report on the very first, critically important step of the project, i.e. the chemical and nanostructural characterization of the starting alumina sample, and the phases resulting from successive incorporation of the lanthana and the Ce/Tb mixed oxide to the alumina support. For this purpose, structural (x-ray diffraction, high-resolution electron microscopy), surface analysis (XPS) and chemical (temperature-programmed desorption mass spectrometry and Fourier transform infrared spectroscopy) characterization techniques have been applied systematically.

EXPERIMENTAL

Pure alumina, Al_2O_3-supported lanthana (La_2O_3/Al_2O_3) and a cerium/terbium mixed oxide supported on lanthana-modified alumina ($Ce_{0.8}Tb_{0.2}O_x/La_2O_3/Al_2O_3$) have been investigated.

The alumina is a commercial sample, kindly provided by Kondea. Prior to its use as a support, the sample was calcined in air at 1023 K for 4 h.

The La_2O_3/Al_2O_3 sample was prepared by impregnating the alumina support with an aqueous solution of lanthanum nitrate (1 M, Fluka, 99.9% purity). The incipient wetness impregnation technique was followed. After impregnation, the sample was dried in air at 110 °C for 10 h and calcined at 1023 K in air for 4 h. The lanthana loading was 20 wt.% (20 g La_2O_3 100 g^{-1} alumina).

The ternary system $Ce_{0.2}Tb_{0.8}O_x/La_2O_3/Al_2O_3$ was prepared by dry impregnation of 20% La_2O_3/Al_2O_3 with an aqueous solution containing a mixture of Ce and Tb nitrates (Aldrich, 99.99% purity). The Ce/Tb molar ratio was 80/20. The impregnated sample was dried further in air at 383 K for 10 h and calcined at 973 K for 4 h. The resulting oxide will be labelled as T20C. The loading of the cerium/terbium mixed oxide was 24 g of T20C per 100 g of Al_2O_3. The resulting ternary system will be referred to as $T20C/La_2O_3/Al_2O_3$. The nominal loadings indicated above were confirmed by chemical analysis. For this purpose, the dissolved sample was analysed further by inductively coupled plasma ICP.

Pure lanthana, ceria–terbia (Ce/Tb, 80 : 20) and ceria–lanthana (Ce/La, 80 : 20) mixed oxides were studied as reference samples. The lanthanum oxide was a commercial (99.9% pure) sample from Fluka. Because of the high sensitivity of the lanthanum oxide to the atmospheric H_2O and CO_2, this lanthana sample, which had been stored without any special precautions, actually consisted of a partly carbonated hydroxide;[26] accordingly, it will be referred to as aged-La_2O_3.

The Ce/Tb and La/Ce mixed oxides, with 20% Tb and La molar content, were prepared from appropriate mixtures of 1 M solutions of the corresponding nitrates (99% pure) from Fluka. An excess of concentrated ammonia (p.a. quality from Merck) was used to precipitate the mixed oxide precursors. After washing and drying in air at 383 K for 10 h, the precipitates were calcined in air at 873 K for 2 h. The resulting Ce/Tb and La/Ce mixed oxides will be labelled as T20C and L20C, respectively.

Structural characterization of the samples was performed by x-ray diffraction (XRD) and high-resolution electron microscopy (HREM). The XRD powder diffraction patterns were collected on a Phillips PW 1820 diffractometer by using Cu Kα radiation and an Ni filter. A Jeol JEM-2000-EX electron microscope with a structural resolution of 0.21 nm was used to obtain the HREM images.

Two additional techniques were applied in the chemical characterization studies, Temperature-programmed desorption (TPD) and Fourier transform infrared spectroscopy (FTIR). The analytical device used for the TPD measurements was a mass spectrometer (VG Sensorlab 200D). The helium flow rate was always 60 ml min^{-1} and the heating rate was 10 K min^{-1}. The FTIR spectra were recorded on a Mattson instrument (Model 5020). The samples were previously pressed into pellets in a KBr matrix. To prevent the appearance of the band corresponding to adsorbed water on the KBr matrix, it was first calcined at 973 K and kept at 353 K before use.

The XPS measurements have been performed on an SSX-100 spectrometer equipped with a monochromatized Al K_α x-ray source ($h\nu = 1486.6$ eV), with a 600 μm spot size. The x-ray source power is kept at ~150 W. The oxide samples were pressed into a sample holder devoted to powder analyses. Because they are insulating materials, surface charging effects are very important. Electrostatic charging can be stabilized by mounting a nickel grid ~1–2 mm above the samples and by flooding the sample with a wide beam of low-energy electrons (flood-gun). The data accumulation time lasts typically 120–150 min and the energy resolution corresponds to a full width at half-maximum (FWHM) of 1.1 eV for the Au $4f_{7/2}$ peak. The collected data came from the La 3d, Ce 3d, Ce 4d, Tb 4d, O ls and C ls core levels. Binding energies (BE) are referred to the C ls BE of 284.6 eV (hydrocarbon from contamination) and given with an accuracy of 0.2 eV. To analyse the individual contributions of the La 3d core levels, peak decomposition was carried out by using mixed Gaussian–Lorentzian peaks with a Shirley-type background.

No *in situ* chemical treatments were applied to the samples before recording the photoelectron spectra.

RESULTS AND DISCUSSION

Structural characterization studies

Structural characterization of Al_2O_3, La_2O_3/Al_2O_3 and $T20C/La_2O_3/Al_2O_3$ has been carried out by x-ray

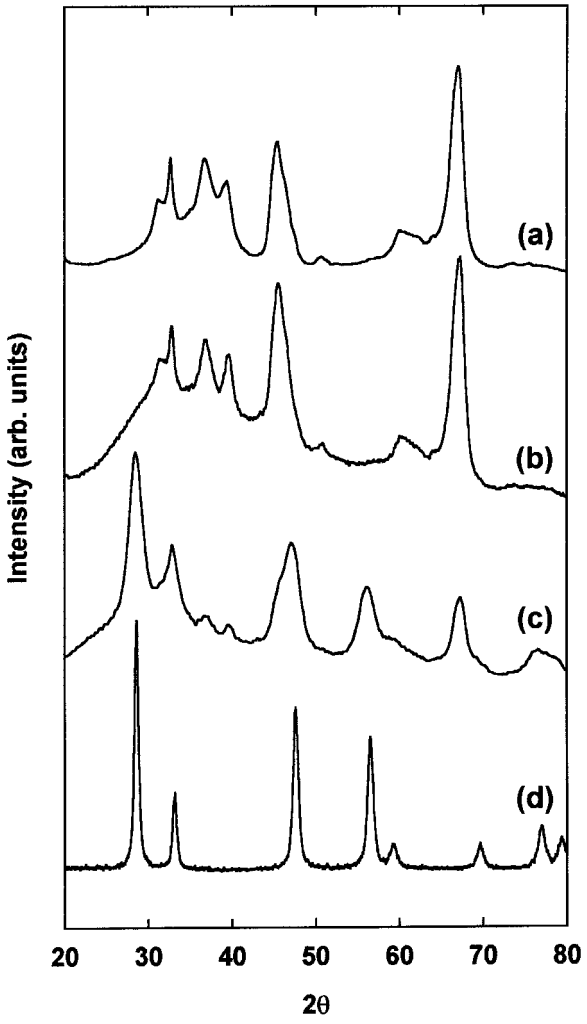

Figure 1. X-ray diffraction patterns corresponding to: (a) Al_2O_3; (b) La_2O_3/Al_2O_3; (c) T20C/La_2O_3/Al_2O_3; (d) T20C (Ce/Tb mixed oxide).

diffraction and HREM. As deduced from Rietveld analysis of the XRD diagrams, the alumina support [Fig. 1(a)] consists of a mixture of crystalline θ and η phases and a third amorphous component. The θ/η ratio was estimated to be 46/54. The presence of the amorphous phase was also confirmed by the HREM images.

The incorporation of lanthana to the transition alumina does not lead to the appearance of any additional diffraction peak, neither attributable to La_2O_3, the phases resulting from their ageing in air,[25] nor to La_2O_3–Al_2O_3 mixed phases.[22] By contrast, as shown in Fig. 1(b), a significant increase of the amorphous contribution to the XRD pattern could be observed. The HREM study [Fig. 2(a)] confirms this observation, the only crystalline phases that could be identified from both the selected area electron diffraction (SAED) patterns and HREM images being the θ and η phases of the Al_2O_3. As an example, Fig. 2(a) shows lattice spacing at 0.46 nm, which has been interpreted as being due to (111) planes of η-Al_2O_3. Also worth noting is that the HREM images do not show areas with enhanced transmission contrasts. Because lanthanum-containing phases should be expected to disperse the electron beam much more effectively than alumina, this observation suggests that the lanthanum-containing phase should actually consist of a highly dispersed two-dimensional amorphous phase supported on the alumina. This proposal, which is consistent with the TPD-MS, FTIR spectroscopy and XPS data to be discussed below, is also in agreement with some earlier studies on the La_2O_3/Al_2O_3 systems.[25] In this respect, it is worth noting that the lanthana loading used here corresponds to a theoretical monolayer of lanthanum oxide covering the whole surface of the alumina support.

Concerning the supported mixed oxide, T20C/La_2O_3/Al_2O_3, XRD [Fig. 1(c)] shows the presence of new diffraction peaks corresponding to a fluorite-like phase. Comparison with the XRD diagram corresponding to the bulk mixed oxide T20C [Fig. 1(d)] shows that the lattice parameter of the fluorite phase in the supported oxide (a_o = 5.442 Å) is slightly larger than that of the bulk oxide of the same nominal chemical composition (a_o = 5.404 Å). This may indicate the presence of trivalent cations in the lattice of the supported oxide, namely Tb^{3+} (cationic radius 118 pm), Ce^{3+} (128.3 pm) or La^{3+} (130 pm). These cations are bigger than the tetravalent Ce^{4+} (111 pm), thus compensating for contraction of the ceria lattice due to the smaller Tb^{4+} cation (102 pm). Also worth noting is the broadness of the diffraction peaks. This suggests that the supported mixed oxide consists of small crystallites dispersed on the surface of the support. The HREM images confirm this proposal. Figure 2(b) shows some small, mixed oxide crystallites. As deduced from a statistical analysis of the micrographs, the average size of these T20C crystallites is ~5 nm.

Chemical characterization studies

Because no direct information about the lanthanum-containing phase could be obtained from the XRD and HREM studies, we have performed some additional characterization experiments, the major aim of which was an investigation of its chemical behaviour. With this purpose, the La_2O_3/Al_2O_3 sample was studied by means of TPD-MS and FTIR spectroscopy. The experiments were run on the stabilized-in-air samples without any further pretreatment. Parallel experiments were run on an aged-in-air pure lanthana sample. In this way, the behaviour of both supported and bulk lanthana samples could be compared, and conclusions about their chemical response to the atmospheric H_2O and CO_2 could be drawn.

Figure 3 reports on the TPD-MS traces for H_2O (m/e: 18) and CO_2 (m/e: 44) corresponding to the stabilized-in-air La_2O_3 (a), Al_2O_3 (b), La_2O_3/Al_2O_3 (c) and T20C/La_2O_3/Al_2O_3 (d). In accordance with several earlier studies,[25] upon exposure to atmospheric H_2O and CO_2, at 298 K lanthana thoroughly transforms into a partly carbonated hydroxide, the final stabilized-in-air oxide actually consisting of a nucleus of crystalline $La(OH)_3$ surrounded by a few layers of a heavily disordered hydroxycarbonate phase. The profiles recorded for lanthana [Fig. 3(a)] fully agree with those reported in the earlier studies commented on above.[25] Accordingly, the following thermal decomposition scheme may be suggested:

$$\begin{array}{ccccccc} La(OH)_3 & & \rightarrow & & LaO(OH) & & \rightarrow & & La_2O_3 & & \rightarrow & & La_2O_3 \\ La(OH)_x(CO_3)_y & \downarrow & & La_2O_2CO_3 & & \downarrow & & La_2O_2CO_3 & & \downarrow & & \\ & H_2O & & & & H_2O & & & & CO_2 & & \end{array}$$

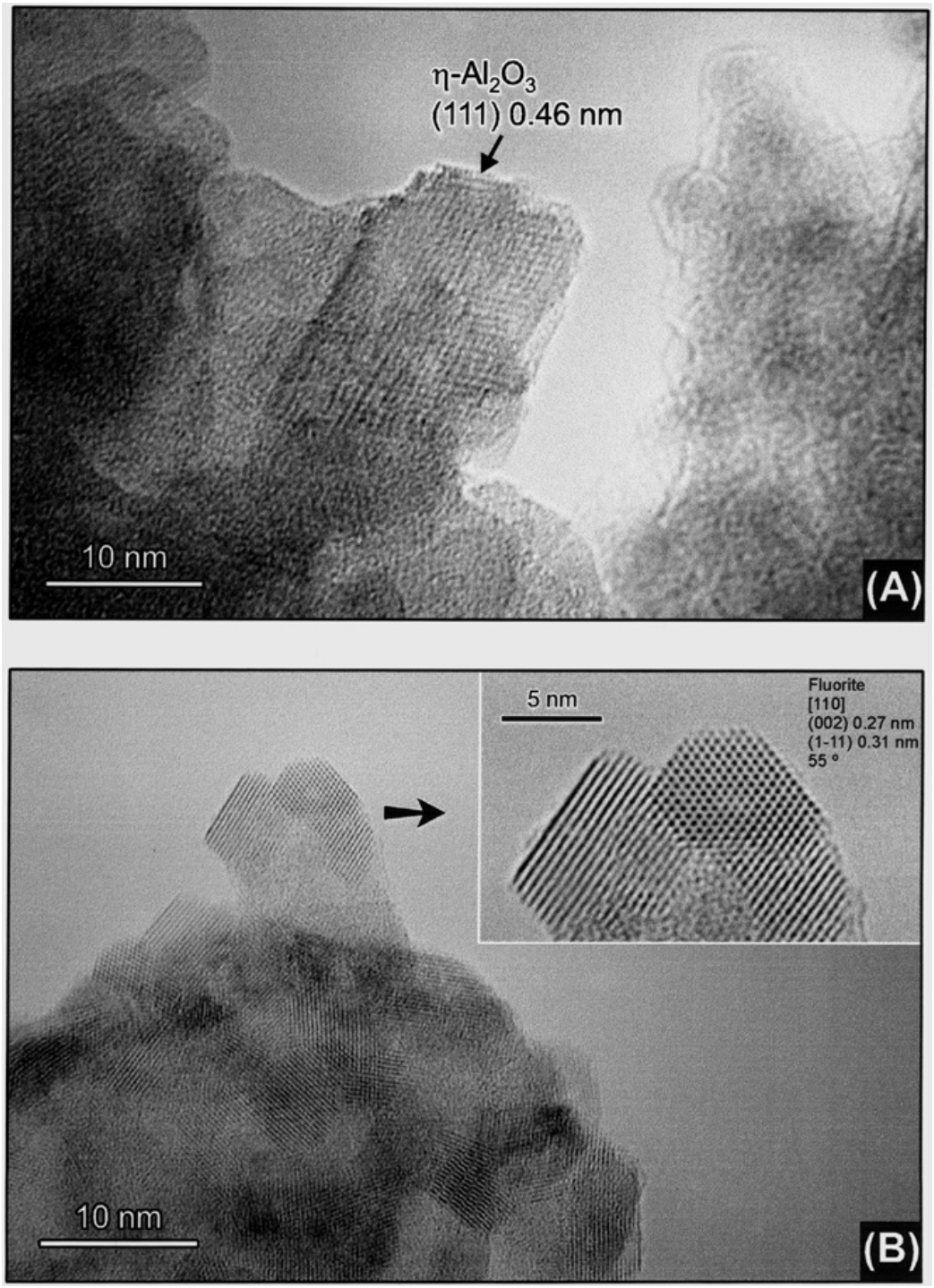

Figure 2. High-resolution electron microscopy images corresponding to La_2O_3/Al_2O_3 (a) and T20C/La_2O_3/Al_2O_3 (b).

As deduced from Fig. 3(c), the lanthana-modified alumina sample behaves in a quite different way; the trace for H_2O consists of a single peak, the maximum of which appears at far lower temperature than those corresponding to the dehydration of the bulk oxide. Likewise, CO_2 desorption takes place through a rather broad peak whose maximum is also strongly shifted to lower temperatures with reference to that observed in this bulk lanthana. Therefore, we may conclude, as already outlined, that supported lanthana behaves quite differently than the bulk oxide, which is consistent with the suggested model, in accordance with which the supported oxide would actually consist of a highly dispersed, raft-like phase.

The FTIR spectra reported in Fig. 4 are also in agreement with this proposal. Thus the ν_{OH} region of the spectrum for aged-in-air bulk lanthana is dominated by a strong narrow peak at 3605 cm^{-1}, which is well known to be characteristic of $La(OH)_3$.[26–28] This feature is completely lacking in the lanthana-containing supported systems. Significant differences may be noted also in the region corresponding to the asymmetric stretching modes of carbonates: 1300–1600 cm^{-1}.

The incorporation of the Ce/Tb mixed oxide to the previous system does not seem to modify strongly the interaction of the sample with H_2O and CO_2 [Figs 3(d) and 4(d)], the only significant difference being the slightly

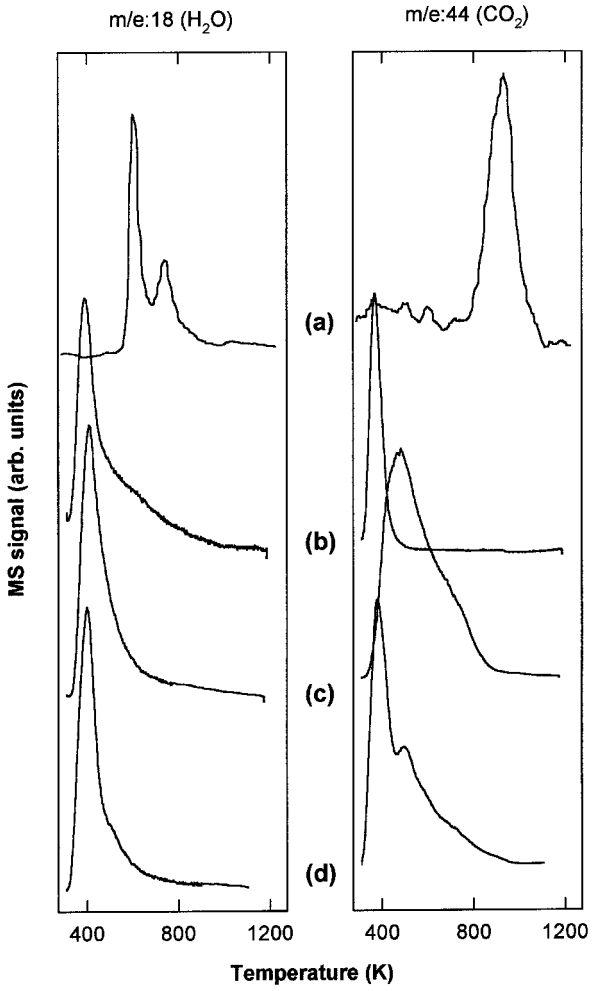

Figure 3. Temperature-programmed desorption traces corresponding to water (*m/e*: 18, left plot) and CO_2 (*m/e*: 44, right plot) evolution from: (a) aged-La_2O_3; (b) Al_2O_3; (c) La_2O_3/Al_2O_3; (d) T20C/La_2O_3/Al_2O_3.

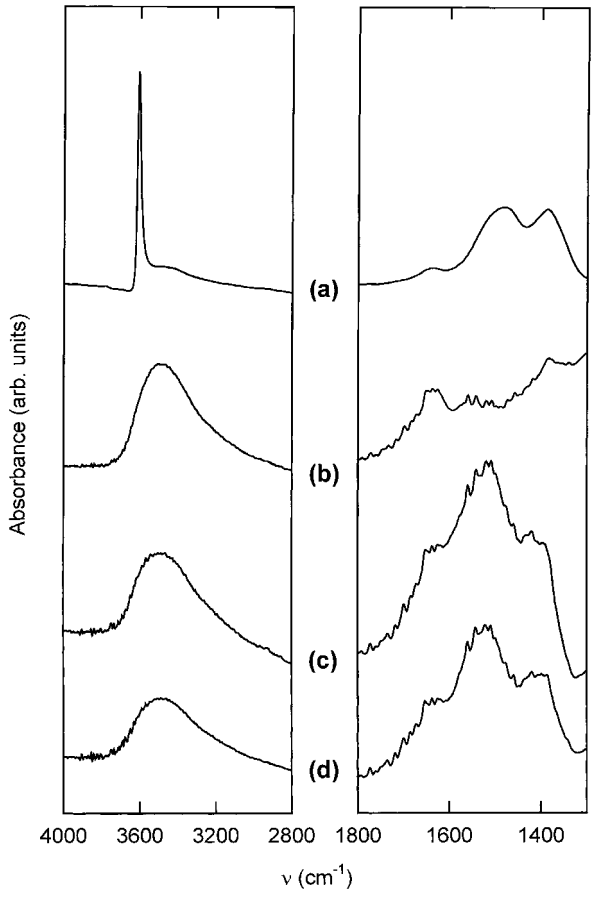

Figure 4. Fourier transform infrared spectra corresponding to: (a) aged-La_2O_3; (b) Al_2O_3; (c) La_2O_3/Al_2O_3; (d) T20C/La_2O_3/Al_2O_3.

smaller amount of H_2O and CO_2 desorbed from the ternary oxide system.

To summarize, the XRD, HREM, TPD and FTIR studies allow us to suggest a model for the T20C/La_2O_3/Al_2O_3 system consisting of three-dimensional crystallites of a fluorite-like ceria/terbia mixed oxide supported on a two-dimensional lanthanum-containing phase covering the alumina surface. As we shall discuss below, this model could be refined further with the help of XPS characterization studies performed on Al_2O_3, La_2O_3/Al_2O_3, T20C/La_2O_3/Al_2O_3, and a series of reference systems including aged-lanthana and two cerium-containing mixed oxides (Ce/La and Ce/Tb) with fluorite structure.

X-ray photoelectron spectroscopy characterization studies

Very few XPS studies of lanthanides are available in the literature. Sarma and Rao[29] applied XPS to the investigation of a wide series of metal oxides, including numerous elements and some rare earths. Among the latter, some oxides relevant to this work were studied: CeO_2, TbO_2, La_2O_3 and Tb_2O_3. The XPS data for CeO_2 were also reported by Wuilloud *et al.*[30] and Fujimori.[31] All these spectra are very complex. Consequently, their interpretation has required extensive theoretical work. An important part of this theoretical effort has been focused on CeO_2. In some other oxides, like lanthana, the 3d core-level spectrum is much simpler.[32] To explain the spectra, both initial- and final-state effects must be considered. In the ground state, the oxygen 2p valence band is completely filled and the La 4f level is empty. More exactly, there is a weak hybridization between the valence band and the 4f state but the energy separation Δ (charge-transfer energy) between the 4f level and the valence band is much larger than the hybridization strength V, so that this latter effect is almost negligible. In the final state of the photoemission process a 3d core electron is removed and the 4f level is pulled down because of the attraction of a core-hole potential U_{fc}. Because Δ and U_{fc} for La_2O_3 are of the same order of magnitude, the energy separation between the 4f level and the valence band becomes very small and a strong hybridization occurs in the final state. This gives rise to two photoemission peaks of comparable energy. With an Al K_α source, it is possible to study the La 3d core level (highest cross-section). On going from La_2O_3 to Ce_2O_3, the intensity ratio of the two peaks changes as the effect of the covalency hybridization is different (Δ and V), but still two photoemission peaks are visible.

A similar covalency hybridization exists in the initial state of CeO_2.[33] The Ce 4f level is located near the top of the O 2p valence band so that the $4f^0$ configuration is strongly mixed with the charge-transfer state $4f^1\underline{L}$, where $\underline{L}$ denotes a hole in the O 2p valence band. In the final state of XPS, the 4f level is pulled down by the core hole potential and the charge transfer occurs from the O 2p to Ce 4f states. Therefore, three doublets due to

configurations $3d4f^0$, $3d4f^1L$ and $3d4f^2L^2$ ($3d$ being a 3d core hole) are observed. In the photoemission of these 3d core levels, one has to take the multiplet splitting effect into account, which is not strong enough to be observed as separate peaks but it contributes to their spectral broadening.

The XPS study has provided quantitative information about the La_2O_3 dispersion in the La_2O_3/Al_2O_3 system by integrating (Eqn (1)) for the Al 2p core level for aluminum in Al_2O_3, λ can be calculated by applying Seah and Dench's formalism[34] for inorganic compounds. The results are given in Table 1.

Using these values, we can estimate an La_2O_3 layer in La_2O_3/Al_2O_3 of $\sim$3.5 Å, which is equivalent to a monolayer. This value gives further support to the model advanced on the basis of XRD, HREM and chemical data, in accordance with which lanthana consists of a highly dispersed bidimensional phase covering the alumina surface.

Figure 5 shows O 1s core-level spectra for a series of oxide samples relevant to this work. These spectra were all recorded on the stabilized-in-air samples without any further thermal pretreatment. The most interesting comparison can be done with the apparent maximum of the peak in each case: pure alumina [Fig. 5(a)] as well as aged lanthana [Fig. 5(b)] present one broad peak at high binding energy (531.1 $\pm$ 0.2 eV). They both correspond to highly hydroxylated, possibly hydrated or carbonated species, which is in good agreement with the TPD-MS and FTIR data. Knowing these reference data for the pure oxides, we analysed the La_2O_3/Al_2O_3 sample [Fig. 5(c)]. The O 1s core-level spectrum is dominated by a broad peak at high BE (530.9 eV), as for the pure oxides. The bulk Ce/Tb mixed oxide [Fig. 5(d)] presents two apparent maxima, one at lower binding energies ($\sim$529.0 eV) and the other on the high binding energy side (+3 eV). In a very recent work,[35] a monocrystalline $CeO_2(001)$ surface was reported to exhibit one single peak at 530.4 eV assigned to the lattice oxygen in CeO_2. In Ref. 36 the spectrum for Ce_2O_3 is reported, consisting of a single peak at 530.7 eV. Accordingly, the low binding energy peak in the Ce/Tb oxide spectrum may be assigned to oxygen species in the bulk oxide lattice, i.e. O^{2-} in the Ce/Tb mixed oxide. We attribute the broad peak at higher binding energy to hydroxyl and carbonate groups chemisorbed on the oxide. In this respect it is worth recalling that the oxide was not submitted to any cleaning routine before recording the spectrum. We have always observed these two features in the XPS analyses of powders of pure ceria or of Ce/Zr[36] and Ce/La mixed oxides. In the case of the $T20C/La_2O_3/Al_2O_3$ supported mixed oxide, [Fig. 5(e)], in addition to the main feature at 531.1 eV, one can detect a pronounced shoulder in the O 1s core level at low BE (528.8 eV) corresponding to oxygen in the lattice of an oxide (as observed for T20C in Fig. 5(d)). It may be linked to the oxygen in the Ce/Tb mixed oxide crystallites previously identified by XRD and HREM. However, the main peak still corresponds to that at high BE observed in La_2O_3/Al_2O_3. Further decomposition of the peaks on the high BE side of all the O 1s core levels would be extremely debatable. Hence, it is difficult to quantify the number of different oxygen environments in alumina or lanthana. Nevertheless, the significant shoulder in the spectra of $T20C/La_2O_3/Al_2O_3$, which is absent in La_2O_3/Al_2O_3 and Al_2O_3 samples, may reasonably be associated with the oxygen in the mixed oxide lattice.

The Al 2p core level [Figs 6(a)–(c)] shows an unresolved doublet at 73.6 eV in the three Al-containing samples (pure Al_2O_3, La_2O_3/Al_2O_3 and $T20C/La_2O_3/Al_2O_3$). This is lower than the BE of Al^{3+} in alumina (amorphous or gamma) proposed by Dufresne *et al.*[37] at 74.8 eV. However, it is possible to find a very large range of BEs from

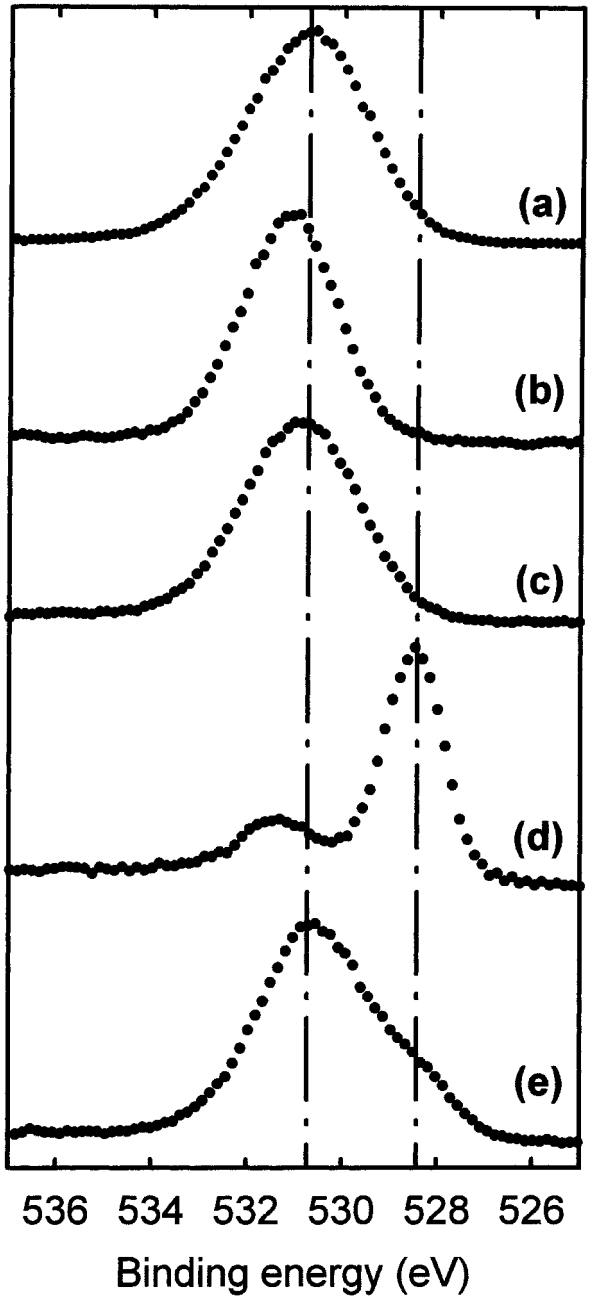

Figure 5. Comparisons of the O 1s core-level peaks in different compounds: (a) Al_2O_3l; (b) aged-La_2O_3; (c) La_2O_3/Al_2O_3; (4) T20C; (5) $T20C/La_2O_3/Al_2O_3$.

Table 1. Mean free paths $\lambda_{Al\ 2p}$ and $\lambda_{La\ 3d}$ calculated with Seah and Dench's formalism

	λ (Å)	$\lambda \sin\theta$ (Å)
Al 2p/Al_2O_3	25.0	14.3
La 3d/La_2O_3	23.7	13.6
La 3d/$La_2(CO_3)_3 \cdot 8\ H_2O$	18.5	10.6

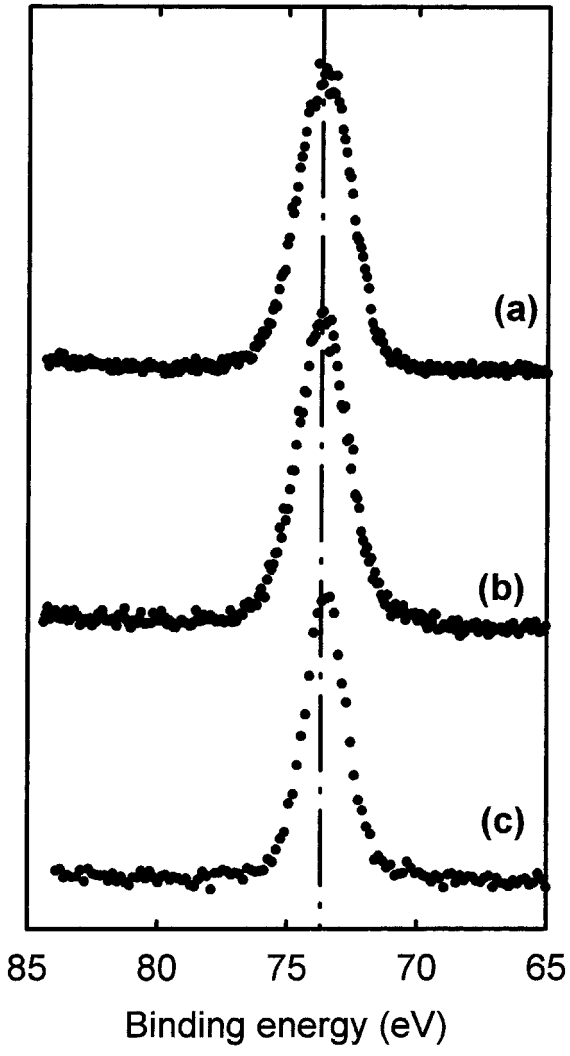

Figure 6. Comparisons of the Al 2p core-level peaks in different oxide compounds: (a) Al_2O_3; (b) La_2O_3/Al_2O_3; (c) T20C/La_2O_3/Al_2O_3.

73.7 to 74.8 eV[38] for the Al 2p core level in alumina. The similarity of the three Al 2p core-level peaks in all the studied samples may be interpreted as an indication of the absence of true mixed oxide phases involving the alumina and either lanthana or, much less likely, ceria and/or terbia. This suggestion is also supported by the XRD and HREM studies, in accordance with which no evidence of lanthanum aluminate can be seen.

The La $3d_{5/2}$ peak (Fig. 7) in aged-La_2O_3 is located at 835.1 eV, with a satellite peak of slightly lower intensity than the main peak but at 3.5 eV higher BE. The spectrum is similar to that for La_2O_3/Al_2O_3 (satellite at 3.2 eV). Shelef *et al.*[39] have reported very similar findings on a lanthana thin film. They interpret the recorded spectrum as being due to a lanthanum carbonate. In their case, however, the satellite intensity was higher than the core-level peak. In this work, the attribution to a lanthanum carbonate is also consistent with the binding energy for the broad O 1s peak.

The La $3d_{5/2}$ spectrum for $Ce_{0.8}La_{0.2}O_{1.9}$ shows remarkable differences with respect to those recorded for La_2O_3 and La_2O_3/Al_2O_3. We find the La $3d_{5/2}$ core level at 833.4 eV (satellite at 4.3 eV). This value is close to the 833.2 eV reported for pure clean lanthanum oxide,[40] i.e.

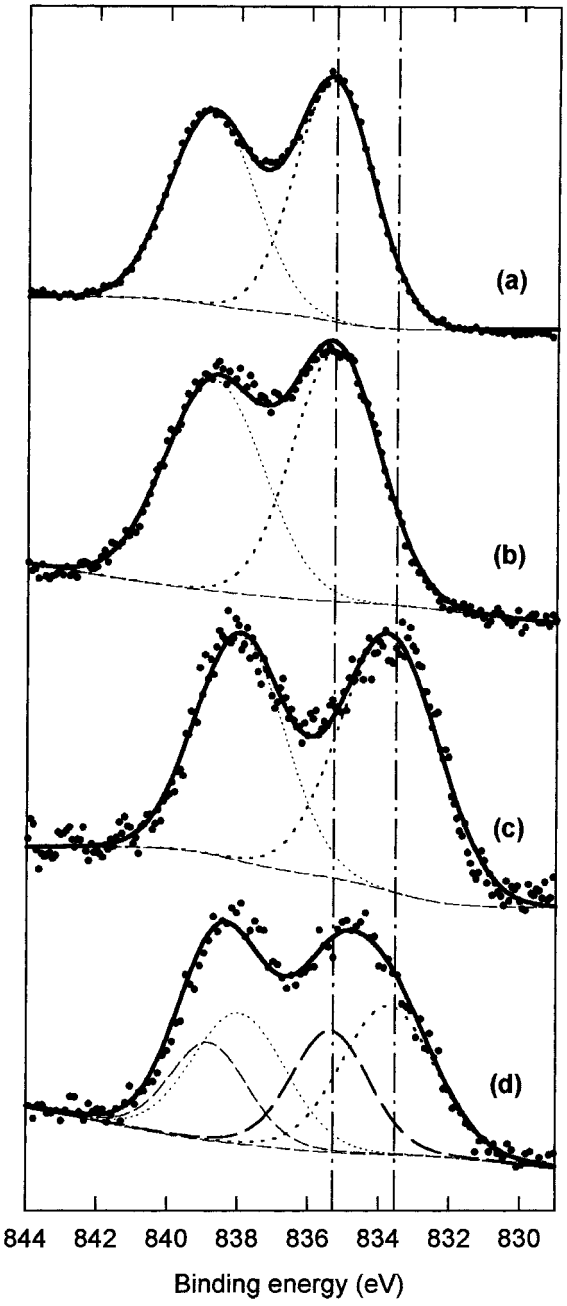

Figure 7. Comparisons of the La $3d_{5/2}$ core-level peaks in different oxide compounds: (a) aged-La_2O_3; (b) La_2O_3/Al_2O_3; (c) L20C (Ce/La mixed oxide); (d) T20C/ La_2O_3/Al_2O_3.

the oxide free from hydroxyl or carbonate species. Also, the similarity of the binding energies recorded for La $3d_{5/2}$ in a fluorite-like oxide lattice (as in $Ce_{0.8}La_{0.2}O_{1.9}$ mixed oxide) and in a hexagonal lattice of pure La_2O_3 is worth noting. By contrast, the shift (−1.7 eV) between the BE of La in the Ce/La mixed oxide relative to the aged-La_2O_3 indicates a significant change in chemical environments for the La^{3+} ions. In this respect, it may be recalled that aged-La_2O_3 actually consists of partially carbonated hydroxide. In T20C/La_2O_3/Al_2O_3, the main La $3d_{5/2}$ peak is located at 834.4 eV (satellite at 3.4 eV), which is intermediate between the binding energies attributed to lanthanum carbonate (835.1 eV) and lanthanum oxide (833.4 eV), respectively. The intensity ratio of the main peak to the satellite is ∼1. However, the shape of the peak is broadened towards the low BE side. By using

the previous BE as references for peak decomposition, we obtained the fit shown in Fig. 7(d). The spectrum is fitted by two peaks at 835.1 eV and 833.4 eV, each being accompanied by a satellite. Accordingly, we may suggest the existence of two kinds of chemical environment for La^{3+}. One of them may be attributed to the hydrated/carbonated highly dispersed La_2O_3. The second one, resembling the spectrum of La^{3+} in an oxide environment, which is specifically associated with the presence of the Ce/Tb mixed oxide, should be interpreted as a strong indication of the incorporation of part of the supported lanthanum to the mixed oxide. This proposal is also consistent with the shift observed in the main XRD peak due to the supported Ce/Tb mixed oxide with reference to that of the bulk mixed oxide with the same nominal chemical composition. An alternative interpretation, allowing us to justify the observation of La^{3+} signals attributable to an oxide environment, would consist of assuming the formation of $LaAlO_3$ oxide at the surface. This hypothesis seems to be much less plausible because we have no evidence of such a phase in La_2O_3/Al_2O_3, the temperature used for preparing the T20C/La_2O_3/Al_2O_3 supported oxide being lower than that previously applied to prepare the supported lanthana sample.

To summarize the XPS contribution to the characterization of the ternary system T20C/La_2O_3/Al_2O_3, the O 1s core level presents two peaks: one is attributed to the presence of the support (La_2O_3/Al_2O_3); the other one at lower BE corresponds to oxygen in the lattice of an oxide, such as T20C mixed oxide. Comparative analysis of the Al 2p core level does not allow us to distinguish any difference in the chemical environment of Al^{3+} in the transition alumina, La_2O_3/Al_2O_3 or T20C/La_2O_3/Al_2O_3. In all the cases, the BE is the same and corresponds to aluminum oxide. This is in agreement with previous XRD and HREM analyses, where no lanthanum aluminate phase could be detected. By using as references the BEs determined for aged-La_2O_3/Al_2O_3 and the Ce/La (L20C) mixed oxide, the peak decomposition of the La 3d core level of the T20C/La_2O_3/Al_2O_3 shows the distribution of La^{3+} between these two types of chemical environments: one of them is similar to that observed in the aged-in-air La_2O_3 and La_2O_3/Al_2O_3 samples, being consistent with a heavily hydrated and carbonated phase; the second one may be attributed to a true oxide environment like the one found in the fluorite-like cerium/lanthanum mixed oxide. As shown in Refs 17 and 41, this oxide does not undergo bulk hydration and carbonation phenomena and therefore is free from the aging effects observed in pure lanthana.

CONCLUSION

Chemical interaction of lanthana and Ce/Tb mixed oxide with the alumina support shows remarkable differences. The former spreads over the alumina, whereas the latter leads to the formation of a well-defined crystalline supported oxide phase showing a fluorite-like structure.

Under the experimental preparation conditions applied in this work, at least a fraction of the supported lanthana is sufficiently labile as to allow its incorporation to the Ce/Tb mixed oxide, thus leading to a Ce/La/Tb mixed oxide. The presence of lanthana in the mixed oxide may significantly influence its redox properties, being therefore a relevant characterization data when analysing the behaviour as a component of Three Way Model Catalysts. Because lanthana is often added in many formulations of TWCs, the occurrence of phenomena like those reported here may also be relevant in the interpretation of the properties of ceria-containing fluorite-like materials for TWC applications.

Acknowledgements

This work has been partly supported by the TMR Programme of the EU under contract ERB FMRX-CT96-0060 (CEZIRENCAT Project). R.S. acknowledges support from the Belgian Fund for Scientific Research (FNRS).

REFERENCES

1. Trovarelli A. *Catal. Rev. Sci. Eng.* 1996; **38**: 439.
2. Trovarelli A, de Leitenburg C, Boaro M, Dolcetti G. *Catal. Today* 1999; **50**: 353.
3. Taylor KC. *Catal. Rev. Sci. Eng.* 1993; **35**: 457.
4. Harrison B, Diwell AF, Hallett C. *Platinum Met. Rev.* 1988; **32**: 73.
5. Diwell AF, Rajaram RR, Shaw HA, Truex TJ. *Stud. Surf. Sci. Catal.* 1991; **71**: 139.
6. Fornasiero P, di Monte R, Rao GR, Kaspar J, Meriani S, Trovarelli A, Graziani M. *J. Catal.* 1995; **151**: 168.
7. Zamar F, Trovarelli A, de Leitenburg C, Dolcetti G. *J. Chem. Soc., Chem. Commun.* 1995; 965.
8. Yao HC, Yao YFY. *J. Catal.* 1984; **86**: 254.
9. Balducci G, Fornasiero P, di Monte R, Kaspar J, Meriani S, Graziani M. *Catal. Lett.* 1995; **33**: 193.
10. Fornasiero P, Balducci G, di Monte R, Kaspar J, Sergo V, Gubitosa G, Ferrero A, Graziani M. *J. Catal.* 1996; **164**: 173.
11. Baker RT, Bernal S, Blanco G, Colón G, Kaspar J, Pijolat M, Pintado JM, Vidal H. *Catal. Today*, in press.
12. Otsuka-Yao S, Morikawa H, Izu N, Okuda K. *J. Jpn. Inst. Met.* 1995; **59**: 1237.
13. Fornasiero P, Kaspar J, Graziani M. *J. Catal.* 1997; **167**: 576.
14. Baker RT, Bernal S, Blanco G, Cordón A, Pintado JM, Rodríguez-Izquierdo JM, Fally F, Perrichon V. *Chem. Commun.* 1999; 149.
15. Pijolat M, Prin M, Soustelle M, Touret O, Nortier P. *Stud. Surf. Sci. Catal.* 1995; **96**: 325.
16. Pijolat M, Prin M, Soustelle M, Touret O, Nortier P. *J. Chem. Soc. Faraday Trans.* 1995; **91**: 3941.
17. Bernal S, Blanco G, Cauqui MA, Cifredo G, Pintado JM, Rodríguez-Izquierdo JM. *Catal. Lett.* 1998; **53**: 51.
18. Logan AD, Shelef M. *J. Mater. Res.* 1994; **9**: 468.
19. Sinev MY, Graham GW, Haack LP, Shelef M. *J. Mater. Res.* 1996; **11**: 1960.
20. Bernal S, Blanco G, Cauqui MA, Corchado P, Pintado JM, Rodríguez-Izquierdo JM, Vidal H. *Stud. Surf. Sci. Catal.* 1998; **116**: 611.
21. Bernal S, Blanco G, Cauqui MA, Corchado P, Pintado JM, Rodríguez-Izquierdo JM. *Chem. Commun.* 1997; 1545.
22. Alvarez LJ, Fernández Sanz J, Capitán MJ, Odriozola JA. *J. Mol. Struct. (Theochem)* 1993; **287**: 161.
23. Subramanian S, Kudla RJ, Peters CR, Chattha MS. *Catal. Lett.* 1992; **16**: 323.
24. Miki T, Ogawa T, Haneda M, Kakuta N, Ueno A, Tateishi S, Matsuura S, Sato M. *J. Phys. Chem.* 1990; **94**: 6464.
25. Bernal S, Botana FJ, García R, Rodríguez-Izquierdo JM. *React. Solids* 1987; **4**: 23.
26. Bernal S, Díaz JA, García R, Rodríguez-Izquierdo JM. *J. Mater. Sci.* 1985; **20**: 537.
27. Rosynek MP, Magnuson DT. *J. Catal.* 1977; **46**: 402.

28. Vannice MA, Klingenberg B. *Chem. Mater.* 1996; **8**: 2755.
29. Sarma DD, Rao CNR. *J. Electron Spectrosc. Relat. Phenom.* 1980; **20**: 25.
30. Wuilloud E, Delley B, Schneider W-D, Baer Y. *Phys. Rev. Lett.* 1984; **53**: 202.
31. Fujimori A. *Phys. Rev. B* 1984; **28**: 4489.
32. Kotani A, Ogasawara H. *J. Electron Spectrosc. Relat. Phenom.* 1992; **60**: 257.
33. Kotani A, Ogasawara H. *J. Electron Spectrosc. Relat. Phenom.* 1997; **86**: 65.
34. Seah MP, Dench WA. *Surf. Interface Anal.* 1979; **1**: 2.
35. Mullins DR, Overbury SH, Hunsley DR. *Surf. Sci.* 1998; **409**: 307.
36. Galtayries A, Sporken R, Riga J, Blanchard G, Caudano R. *J. Electron Spectrosc. Relat. Phenom.* 1998; **88–91**: 951.
37. Dufresne P, Payen E, Grimblot J, Bonnelle JP. *J. Phys. Chem.* 1981; **85**: 2344.
38. *Handbook of X-ray Photoelectron Spectroscopy.* Perkin-Elmer, Eden Prairie: MN, 1992.
39. Shelef M, Haack LP, Soltis RE, DeVries JE, Logothetis EM. *J. Catal.* 1992; **137**: 114.
40. Haack LP, DeVries JE, Otto K, Chattha MS. *Appl. Catal.* 1992; **82**: 199.
41. Blanco G. PhD Thesis, University of Cádiz, 1997.

